

PAPER

An integrated model of scintillator-reflector properties for advanced simulations of optical transport

To cite this article: Emilie Roncali *et al* 2017 *Phys. Med. Biol.* **62** 4811

View the [article online](#) for updates and enhancements.

Related content

- [Advanced optical simulation of scintillation detectors in GATE V8.0: first implementation of a reflector model based on measured data](#)
Mariele Stockhoff, Sébastien Jan, Albertine Dubois *et al.*
- [Simulation of light transport in scintillators based on 3D characterization of crystal surfaces](#)
Emilie Roncali and Simon R Cherry
- [Predicting the timing properties of phosphor-coated scintillators using Monte Carlo light transport simulation](#)
Emilie Roncali, Jeffrey P Schmall, Varsha Viswanath *et al.*

Recent citations

- [Modelling the transport of optical photons in scintillation detectors for diagnostic and radiotherapy imaging](#)
Emilie Roncali *et al*

Quantify 3D Geometric Distortion in MR Images

Verify the accuracy of target delineation and treatment efficacy for MRgRT



Watch Video

modusQA
Accuracy. Confidence.™

An integrated model of scintillator-reflector properties for advanced simulations of optical transport

Emilie Roncali, Mariele Stockhoff and Simon R Cherry

Department of Biomedical Engineering, University of California Davis, Davis, CA,
United States of America

E-mail: eronicali@ucdavis.edu

Received 17 March 2017, revised 31 March 2017

Accepted for publication 11 April 2017

Published 18 May 2017



CrossMark

Abstract

Accurately modeling the light transport in scintillation detectors is essential to design new detectors for nuclear medicine or high energy physics. Optical models implemented in software such as Geant4 and GATE suffer from important limitations that we addressed by implementing a new approach in which the crystal reflectance was computed from 3D surface measurements. The reflectance was saved in a look-up-table (LUT) then used in Monte Carlo simulation to determine the fate of optical photons. Our previous work using this approach demonstrated excellent agreement with experimental characterization of crystal light output in a limited configuration, i.e. when using no reflector.

As scintillators are generally encapsulated in a reflector, it is essential to include the crystal-reflector interface in the LUT. Here we develop a new LUT computation and apply it to several reflector types. A second LUT that contains transmittance data is also saved to enable modeling of optical crosstalk.

LUTs have been computed for rough and polished crystals coupled to a Lambertian (e.g. Teflon tape) or a specular reflector (e.g. ESR) using air or optical grease, and the light output was computed using a custom Monte Carlo code. $3 \times 3 \times 20 \text{ mm}^3$ lutetium oxyorthosilicate crystals were prepared using these combinations, and the light output was measured experimentally at different irradiation depths. For all reflector and surface finish combinations, the measured and simulated light output showed very good agreement.

The behavior of optical photons at the interface crystal-reflector was studied using these simulations, and results highlighted the large difference in optical properties between rough and polished crystals, and Lambertian and specular reflectors. These simulations also showed how the travel path of individual scintillation photons was affected by the reflector and surface finish.

The ultimate goal of this work is to implement this model in Geant4 and GATE, and provide a database of scintillators combined with a variety of reflectors.

Keywords: scintillation detectors, light transport, optical Monte Carlo, GATE, Geant4, surface finish, diagnostic imaging

(Some figures may appear in colour only in the online journal)

1. Introduction

Accurately modeling the light transport in scintillation detectors is a key requirement for scientists who are designing new detectors for nuclear medicine, high energy physics experiments, or homeland security applications. In the field of positron emission tomography (PET) in particular, there is a major effort to develop ultra-high timing resolution detectors for time-of-flight (TOF). Achieving a timing resolution below 100ps and ultimately 10ps (Nemallapudi *et al* 2015, Gundacker *et al* 2016) requires optimization of every aspect of the detector, including efficient extraction of scintillation light from the crystal (Lecoq 2012, Berg *et al* 2015, Weele *et al* 2015). In long axial field-of-view PET scanners or preclinical systems with tight bore diameters, detectors that encode depth-of-interaction (DOI) have also been developed to correct parallax errors. These detectors often use customized designs with very specific crystal surface treatments (Yang *et al* 2006, Ito *et al* 2013, Roncali *et al* 2014 b) that are optimized with simulations (Ito *et al* 2010). To perform those simulations, optical models have been implemented in the widely distributed opensource software Geant4 (Agostinelli *et al* 2003, Pizzichemi *et al* 2012) and GATE (Cuplov *et al* 2014, Jan *et al* 2004), based on previous work done in DETECT2000 (Levin and Moisan 1996). GATE currently includes the UNIFIED model, which suffers from major limitations that makes anything other than perfectly polished crystals impossible to simulate optically with reasonable accuracy (Janecek and Moses 2010, Roncali and Cherry 2013). Geant4 includes a more realistic model of crystal optical properties developed by Janecek and Moses (2010).

In previous work, we developed a model of crystal reflectance computed from 3D measurements of the crystal surfaces (Roncali and Cherry 2013). This model was tested using custom code and demonstrated excellent agreement with experimental characterization of crystal light output in select detector configurations, such as a crystal without a reflector on its sides, or with a purely Lambertian, air-coupled, reflector. We also obtained very good agreement with the results of Janecek and Moses, who measured the reflectance of bismuth germanate (BGO) using scintillator crystals cut in hemispheres and a dedicated benchtop setup (Janecek and Moses 2009). In both approaches, reflectance properties are saved in a look-up-table (LUT) and used in optical simulation to determine the fate of photons impinging on the crystal faces. In our model, each time a photon interacts with the crystal face at a given angle of incidence, the LUT is used to (1) determine whether this photon is reflected in the crystal and to (2) select the direction of reflection if it is reflected. Our initial model was based on LUTs that included the crystal-outer medium interface but not the reflector, and only considered the simple case of Lambertian reflectors air-coupled to the crystal (e.g. Teflon tape). The LUT itself did not include the reflector model, which was processed as a second step.

As scintillators are generally encapsulated in a reflector, it is essential to include the crystal-coupling-reflector interface in the LUT computation, which is the core of this work. Our ultimate goal is to implement this model in Geant4 and GATE and provide a database of scintillators combined with a variety of reflectors. In the work presented here, we extended

our LUT computation algorithm to include the reflector, the coupling medium, and photon tracking between the two interfaces. In addition to the reflectance LUT, the transmittance and direction of transmitted rays are also saved and used to describe the light traversing through the reflector and its contribution to the neighboring crystals. This is a critical factor to study optical crosstalk in crystal arrays (Loignon-Houle *et al* 2015). Though there are similarities between our work and that of Janecek and Moses (2010), there are also critical differences. First, our model does not rely on a fixed coefficient of reflectivity for the crystal or the reflector but rather computes the reflectivity of each given surface as a function of incidence angle, resulting in a more customized model of a given crystal finish. As shown in our previous work, the reflectivity indeed depends on the incidence of the photons, thus extracting it from the surface will result in a more accurate representation of the surface. Second, their database of surfaces was limited to BGO crystals, and would require new crystal hemispheres to be manufactured to characterize other materials, as the reflectivity depends on the crystal's index of refraction. By using a computational approach to calculate the reflectance properties, only a small sample of a flat crystal surface is needed in our model, making it more flexible and readily expanded to other materials. Third, their work did not include transmittance (Janecek and Moses 2010), which is needed to quantify the contribution of optical cross-talk to neighboring crystals.

The crystal-reflector LUT was first validated against experimental data for a limited set of combinations, and was then applied to compare the angular distribution of the reflected photon directions for a crystal without reflector, a crystal with a pure Lambertian reflector, a pure specular reflector coupled to the crystal with air or attached with optical grease (e.g. ESR, 3 M). A realistic reflector with a mixture of specular and Lambertian reflection (e.g. glossy tape) was also modeled. The resulting light output, travel path length in the crystal, and number of reflections on the crystal sides was also studied and illustrated the effect of both the reflector and crystal surface finish. To our knowledge this is the first time that accurate models of reflectors and crystal surface finish have been combined to characterize optical photon paths within scintillation crystals.

2. Materials and methods

2.1. Reflectance and transmittance of the crystal surface

We briefly summarize the measurement of the crystal surfaces and the computation of the reflectance LUTs. More details can be found in Roncali and Cherry (2013). First, crystal surfaces are characterized with atomic force microscopy with a spatial resolution of 87 nm (typically a $45 \mu\text{m} \times 45 \mu\text{m}$ field-of view scanned in 512×512 pixels). Both the reflection coefficient and the direction of reflected rays are then computed every 1° for angles of incidence varying between 0° and 90° (figure 1), and saved in the reflectance LUT.

To compute the reflection coefficient and direction at each angle of incidence, the 3D surface is virtually illuminated with a collimated light beam. Each photon is tracked to the surface, and its reflection or transmission is determined using Fresnel equations with respect to the local surface. The beam is rotated around the global normal to the surface to ensure sufficient sampling of the different local slopes. The reflectance is computed as the fraction of photons that were reflected. All individual photons reflected back in the crystal are saved in the reflectance LUT. Figure 1(a) shows an example of reflectance computed for polished, etched, and rough surfaces using AFM scanned samples. Our algorithm shows very good agreement with Janecek and Moses' measurements (Janecek and Moses 2009). Figure 1(b) shows the broad angular distribution of the reflected rays for a rough crystal illuminated at 20° .

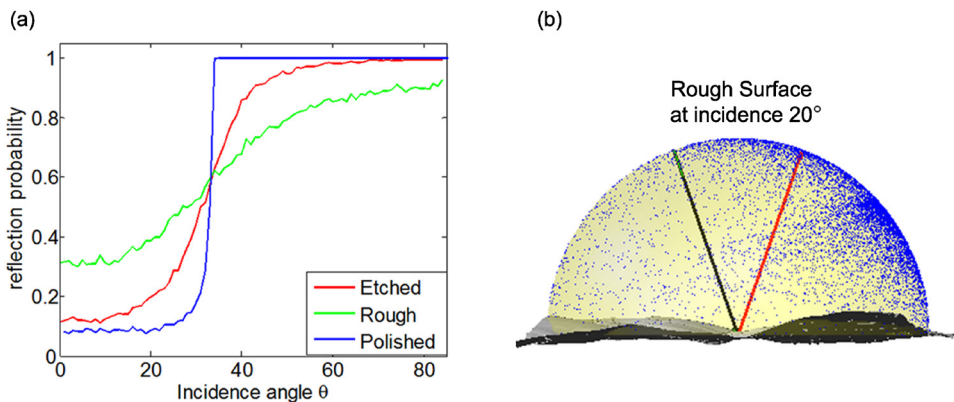


Figure 1. (a) Reflectance probability as a function of incidence angle for rough, etched, and polished crystals without reflector. (b) 3D distribution of reflected rays for a 20° incident light (black) shone on a rough surface without reflector. Specular reflection would follow the red arrow; blue dots indicate the actual reflected rays.

Table 1. Summary of input parameters to compute the LUTs.

Medium	Parameter	Type of variable
Scintillator	Topography (e.g. measured with AFM)	Matrix (e.g. 512×512)
	Refractive index	Scalar
	Scintillation emission spectrum	Vector
Coupling	Refractive index	Scalar
	Bulk absorption (0 by default)	Scalar
Reflector	Type (specular or lambertian)	Name
	Composition as function of incidence angle	Vector
	Reflectivity spectrum	Vector

In this work, we now track the photons that are transmitted through the surface. These photons are first refracted depending on the index of refraction of the crystal and of the coupling medium (e.g. 1 for air, 1.45–1.6 for typical optical glues and optical grease). All photons that cross the reflector interface are saved in the transmittance LUT. For a given surface, two LUTs are saved: the reflectance LUT contains the reflectivity as a function of incidence angle and the angular distribution of reflected rays for each incidence angle, while the transmittance LUT contains transmittance coefficient and the angular distribution of transmitted rays for each incidence angle. The sum of the reflectance and transmittance naturally equals 1.

2.2. Integration of reflector and crystal interface

Photons transmitted through the crystal-coupling interface are tracked until they reach the reflector, and are allowed to reflect back and forth between the reflector and crystal interface (figure 2). When photons cross the reflector, they are saved in the transmittance LUT. When photons enter back in the crystal, their direction is changed to account for refraction and they are saved in the reflectance LUT (in red, figure 2). The ultimate angular distribution of reflected photons is a combination of photons directly reflected by the crystal and photons

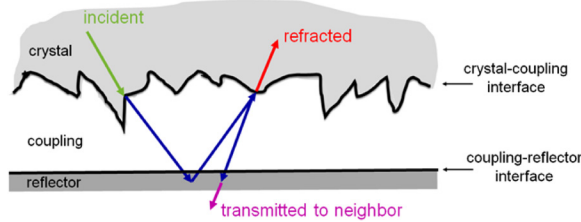


Figure 2. Crystal-reflector interface. The incident photon is shown in green, the refracted photon reflected by the reflector (with possible further reflections at interfaces bordering the coupling medium) is in blue. Photons ultimately transmitted through the reflector are shown in magenta, while photons re-entering the crystal are shown in red.

Table 2. Crystal surface treatment, coupling medium, and reflector type.

Crystal surface treatment	Coupling (n)	Reflector
Rough ($R_a = 0.48 \mu\text{m}$, $\sigma = 0.57 \mu\text{m}$, $R_{pv} = 3.12 \mu\text{m}$) ^a	Air (1)	No reflector
	Air (1)	Lambertian (Teflon 4 layers)
	Grease (1.5)	specular (ESR)
Polished ($R_a = 20.8 \text{ nm}$, $\sigma = 26.2 \text{ nm}$, $R_{pv} = 34.7 \text{ nm}$) ^a	Air (1)	No reflector
	Air (1)	Lambertian (Teflon 4 layers)
	Grease (1.5)	Specular (ESR)

^a R_a = average roughness; σ = rms roughness, R_{pv} = peak-to-valley roughness.

reflected by the reflector that ultimately re-enter the crystal. All interactions at the interfaces between the crystal-coupling medium and coupling medium-reflector are processed using Fresnel equations and Snell's law for unpolarized light. In contrast to the measured crystal topography, the reflector is assumed to be a perfectly flat surface with a constant normal vector equal to the nominal crystal surface normal vector.

The index of refraction of the coupling medium was set at 1 (air), and 1.5 (representative of Bicron BC-630, St Gobain, which was used in the experimental validations). Individual photons propagate in the coupling medium and are tracked until they are either transmitted or re-enter the crystal. The reflector was positioned at a distance equal to the coupling medium thickness, taken from the minimum of the crystal surface. For a rough crystal surface, the typical maximum height variation is $\pm 1.5 \mu\text{m}$ (table 2), which implies that the coupling medium thickness in the simulations is not constant, reflecting realistic conditions. In contrast, a polished crystal surface has a height variation of $\pm 50 \text{ nm}$ which makes the coupling layer more homogeneous.

2.3. Reflector and crystal modeling

The two primary types of reflectors used in PET detectors were modeled in this study. First, a specular reflector (ESR, 3 M) was modeled as air-coupled or coupled to the crystal with optical grease. It is interesting to note that though specular ESR is often given for a 98% reflectivity or above, the reflectivity actually falls rapidly under 400 nm (figure 3(a)) (Park 2012). Second, a Lambertian reflector (Teflon tape) was modeled as air-coupled to the crystal with 4 layers of wrapping that matched the experimental conditions. To demonstrate the effect of the reflector on the light extraction from the crystal, other Teflon (PTFE) materials were also modeled with different number of layers, with reflectivity values taken from measured data (figure 3(b)) (Janecek 2012).

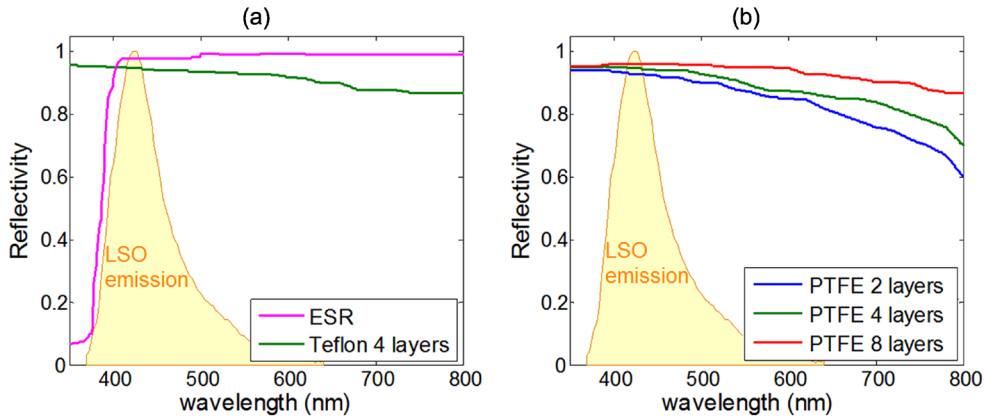


Figure 3. (a) Spectra of reflectors used in the simulations and experiments for validation. Values for the ESR are taken from (Park 2012) and Lambertian reflectors from Janecek (2012). ESR shows a strong wavelength dependency never taken into account in published models and that slightly overlaps with the LSO emission. (b) Other reflectors used in simulations (not included in experiments).

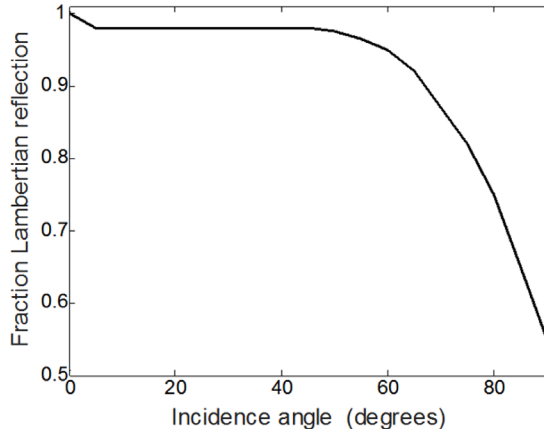


Figure 4. Reflectivity model for glossy tape. At all low incidence angles, the reflector is mostly Lambertian and shows a more specular behavior as the incidence angle increases (~55% at 90°).

Based on values from Janecek and Moses (2008), a reflector with a pure Lambertian behavior (>98%) from 0° to ~50° and a mixed specular/Lambertian behavior from 50° to 90° was created to model Lambertian reflectors with a glossy surface. Figure 4 shows the ratio of Lambertian/specular reflections at each angle of incidence, for a reflector in contact with air.

Table 1 summarizes all input parameters required to compute the LUT.

2.4. Validation against experimental data

2.4.1. Coincidence setup. To validate the computation of the reflectance LUTs integrating the crystal and the reflector, two rough and two mechanically polished $3 \times 3 \times 20 \text{ mm}^3$ lutetium oxyorthosilicate (LSO) crystals were measured. First, the crystals were scanned using AFM to obtain the 3D surfaces used in the optical simulations. Typical roughness parameters

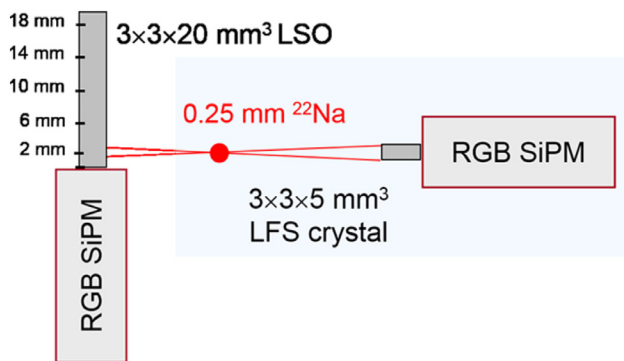


Figure 5. Coincidence setup to measure light output at 2, 6, 10, 14, and 18 mm from the photodetector face. The reference detector is composed of a lutetium fine silicate (LFS) crystal coupled to the RGB SiPM and is moved to obtain data at each depth.

obtained from the measurements are given in table 2: the average roughness R_a is the arithmetic mean of absolute values, while the peak-to-valley roughness R_{pv} is the difference between the maximum and minimum surface height (Ki-Beom *et al* 2003). The polished surface shows much smaller roughness, with values in nm instead of μm for the rough surface. Using these surface samples, we generated reflectance and transmittance LUTs for all configurations listed in table 2. All LUTs were computed with a crystal-reflector coupling layer of 1 μm . When not specified, ‘Teflon’ indicates the Teflon tape with 4 layers shown in figure 3(a).

The rough crystals had five rough sides and one $3 \times 3 \text{ mm}^2$ polished face that was coupled to the photodetector. The polished crystals had all six faces polished. All crystals were coupled to a silicon photomultiplier (SiPM) using optical grease (Bicron BC-630). All crystal surfaces were first cleaned with isopropyl alcohol before being covered with reflector. When using Teflon tape, the crystals were wrapped in 4 layers on all five faces except the face in contact with the photodetector. The ESR was attached in two pieces: one piece covered the long sides of the crystal ($3 \times 20 \text{ mm}^2$) and partially overlapped one of the sides to avoid light leakage along an open edge. The top face was covered with a separate $3 \times 3 \text{ mm}^2$ piece.

The light output of the crystals, defined as the photopeak position, was measured at five different depths using a coincidence setup described in Kwon *et al* (2016). The setup consists of two SiPM (RGB-HD, FBK), one coupled to the crystal of interest and one coupled to a short reference crystal (figure 5). The zero irradiation position is defined as the interface between the photodetector and the crystal. Both detectors were irradiated with a ^{22}Na point source to record 10,000 events at each irradiation depth (figure 5). Accounting for the geometry of the coincidence setup (ratio of distances between the sources and the two detectors) and the size of the point source, we estimate the irradiation to be $\sim 2.5 \text{ mm}$ wide at the crystal surface. The number of detected scintillation photons collected for each event was estimated by integrating the waveform over 1 μs , and the set of all waveform sums was histogrammed at each depth to produce energy spectra. The overall light collection for each detector configuration at each depth was taken as the position of the 511 keV photopeak.

2.4.2. Simulation and tracking of scintillation photons in the crystal. In our previous work we used custom Monte Carlo code to simulate the light output of LSO crystals, and validated it with bare crystals as well as crystals wrapped in Teflon tape (Roncali and Cherry 2013). This custom code simulates gamma interactions at a given position in the crystal and generates a number of scintillation photons proportional to the energy deposited by the gamma interaction and emitted

isotropically. Scintillation photons are then tracked in the crystal until they are detected by the photodetector, or transmitted through the crystal sides, or absorbed in the crystal.

Here, a new version of this custom code that utilizes the crystal-reflector LUTs was used to simulate LSO crystals with an absorption length of 800 nm, a light yield of 35,000 photons per MeV, and an index of refraction of 1.82. The crystal was considered coupled to a photodetector through a layer of optical grease with an index of refraction of 1.5. The photodetector was assumed to have a quantum of efficiency of 1 and a size matching that of the crystal, so that all photons impinging on its sensitive area were detected. This allowed us to collect more photons and maximize the data statistics. Only relative changes in light output were considered to compare experiments and simulations, as absolute quantification of the number of collected photons is not available from the experiments (the actual LSO light yield, the photodetector quantum efficiency, and SiPM saturation, are not known accurately). The scintillator was modeled with a decay time of 40 ns, a rise time of 72 ps, and a broad emission spectrum with a peak at 420 nm (Melcher and Schweitzer 1992, Seifert *et al* 2012). On average, a 511 keV photoelectric interaction produced 17,885 scintillation photons, with each photon given an emission time and wavelength sampled from the time distribution and emission spectrum. Each time a photon hit one surface of the scintillator, the LUT corresponding to the specified surface finish + reflector was used to determine whether the photon was transmitted or reflected, and in which direction.

Emission position, emission time, transit time, travel path in the crystal, number of reflections, wavelength, as well as other parameters were saved for each individual scintillation photon. The output data were used to compute the light collection by forming the energy spectrum and determining the 511 keV photopeak position in a similar way to the experimental data analysis. The optical track lengths (travel path) in the crystal were histogrammed and the distributions for different configurations are reported in sections 3.2.1 and 3.2.2. For all configurations (table 2), 500 gamma interactions were simulated every 4 mm in depth from 2 mm to 18 mm from the photodetector face, with a depth bin width of 2.5 mm to matched that of our experimental setup. Additional configurations were also simulated for a rough crystal combined with reflectors as described in figures 3 and 4: PTFE with 2, 4, or 8 layers, a glossy tape. All reflectors were air-coupled.

3. Results

3.1. Effect of reflector and coupling medium on reflectance and transmittance

3.1.1. Rough crystals. The effect of the various reflectors and reflector-crystal coupling media on reflectivity and transmittance was first compared with the rough crystal (figure 6). The reflectivity for a rough crystal without reflector (solid black curve) sharply rose when the angle of incidence got close to the critical angle (33°). In contrast, the reflectors flattened the curve and did not make a large contribution beyond $\sim 45^\circ$, where most photons underwent reflection by the crystal (figure 6). Reflectivity and transmittance curves for Teflon and ESR were very close, suggesting at first that similar light output could be obtained with crystals of the same size and surface finish (blue and green solid lines, figure 6). However, the angular distribution of the reflected rays for two materials greatly varied, as shown in figure 7 where the rays reflected by the crystal directly are shown by blue dots, while green dots indicate those reflected by the reflector. This illustrates the different angular distributions of Lambertian and specular reflectors; Teflon is Lambertian and spreads the direction of reflected photons over a half sphere, while the specular behavior of ESR directs the reflected rays with an angle close to the incidence angle. This implies that for a photon impinging on the surface with a given incidence angle, the direction of the reflected photon has a strong dependence on the reflector. This will change the travel path of the photon and the subsequent probability of detection. This partially

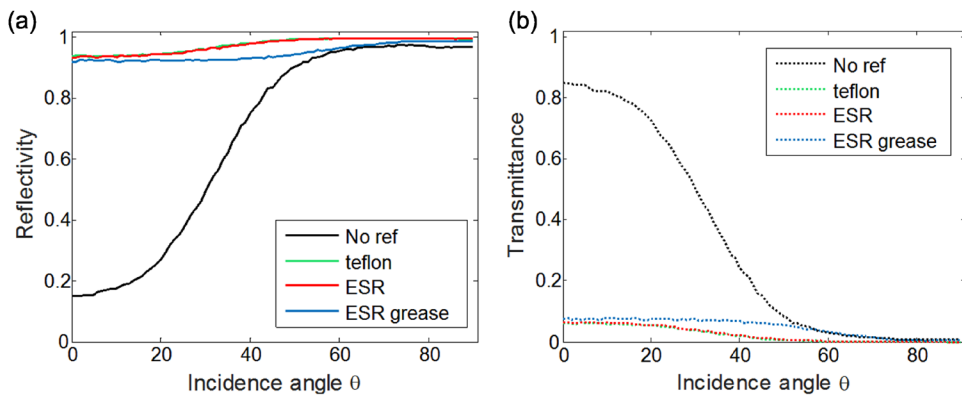


Figure 6. (a) Reflectivity and (b) transmittance for all combinations of rough crystal and reflectors used in experiments. Green, red, and blue curves show a much flatter reflectivity when a reflector is attached to the crystal.

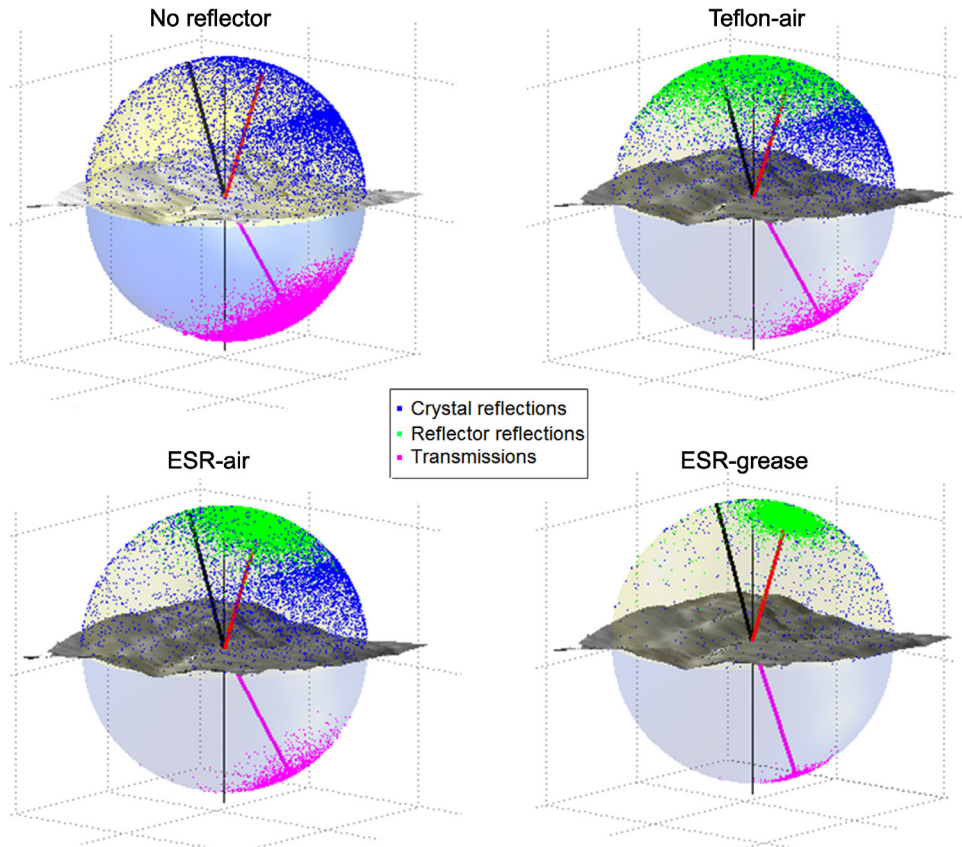


Figure 7. Distribution of reflected and transmitted rays for a rough crystal with no reflector, Teflon, ESR coupled with air and ESR coupled with optical grease (clockwise). Top part represents the crystal space, bottom part the outer medium. The black arrow indicates the incidence angle of 20°; the red arrow shows a perfect specular reflection of the green ray by a flat surface; the magenta arrow shows the refraction of the green ray after the reflector.

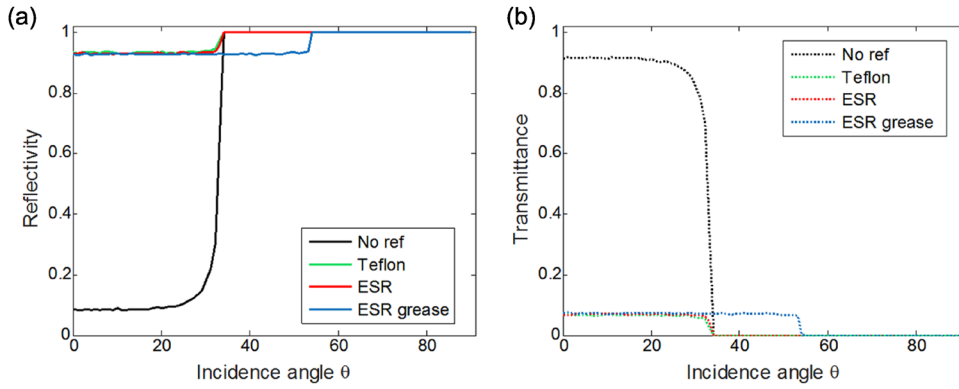


Figure 8. (a) Reflectivity and (b) transmittance for all combinations of polished crystal and reflectors. Polished crystals show a sharper rising edge near the critical angle (33°) than rough crystals.

explains the differences in light output, energy and DOI resolution observed experimentally when using different reflectors (Ren *et al* 2014), and highlights the importance of considering the direction of reflected photons in addition to the probability of reflection.

When optical grease is applied between the ESR and the crystal (a typical detector assembly would favor optical glue for stability but in this validation study we needed to reuse the crystal), the reflectivity decreases as expected: when decreasing the index mismatch between the crystal and the coupling medium, more photons are transmitted through that interface and hit the reflector, some of which may be trapped in the crystal-reflector interface, others will be transmitted through the reflector, or absorbed. Only at very high incidence angles, greater than 75° , does the ESR-grease reflectivity curve approach the ESR-air curve (figure 6). Among the photons that are ultimately reflected, a larger fraction comes from the reflector, as shown in the bottom row of figure 7 (very few crystal reflections are visible).

3.1.2. Polished crystals. The reflectivity curve of the polished surface without reflector (figure 8(a), solid black) showed a sharper rise than the rough crystal (figure 6(a)), following closely the Fresnel equations for an ideal flat surface. This result is consistent with our previous work and that of Janecek and Moses (2009). Similar to the rough crystal, the curves for Teflon and ESR were very close but the angular distribution of reflected rays differed dramatically (figure 9). As expected, ESR reflected the photons in a specular way (see inset ESR-air in figure 9); however the Lambertian nature of Teflon spread the reflected photons over a spherical cap with an angle of 33.33° when refracted back into the crystal. This angle corresponds to the maximum possible angle for refraction from air to LSO ($n_1 = 1$ to $n_2 = 1.82$).

The distribution of ESR-grease reflections was slightly narrower than that of ESR-air, which is due to a higher fraction of photons being reflected in a purely specular fashion by the reflector compared to the air coupling where more photons are reflected by the crystal directly. Although mechanically polished, the crystal surface still contains small local slope variations that spread the reflected rays over a small angular range. This affects the overall reflection pattern in the crystal, especially on the long sides of the crystal, and also the resulting light output.

3.2. Validation of the reflector models

3.2.1. Rough crystals. Figure 10(a) shows the light output as a function of interaction depths. All curves were normalized according to their light output at the 2 mm irradiation position.

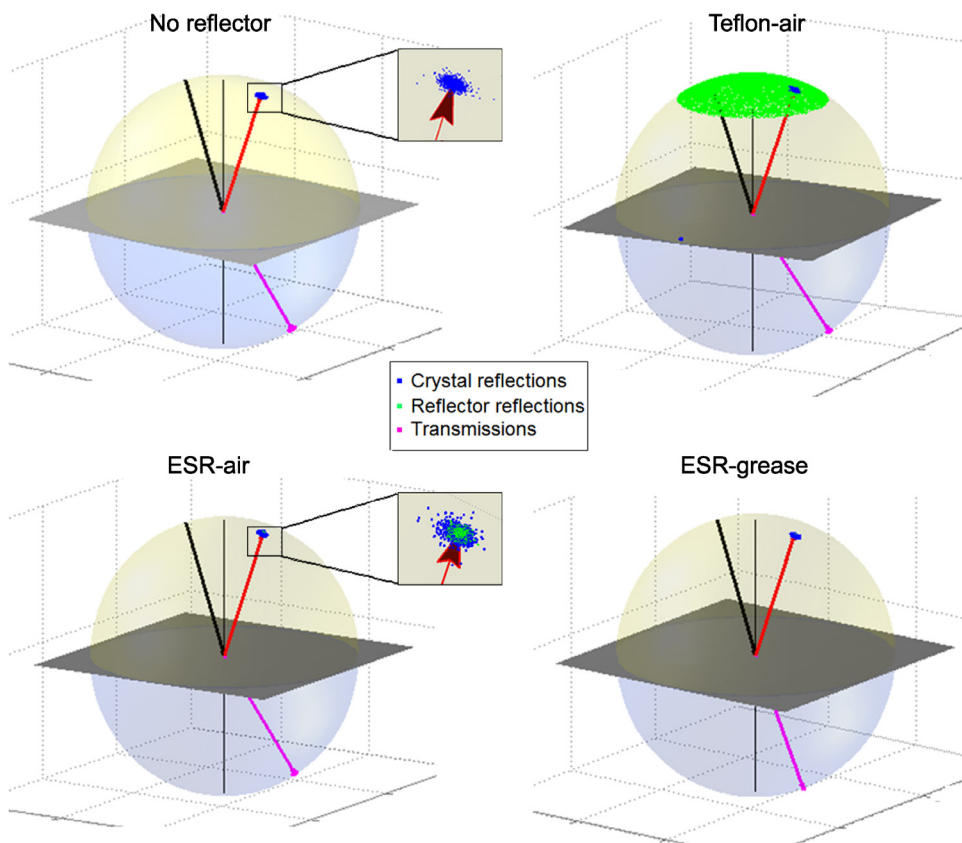


Figure 9. Distribution of reflected and transmitted rays for a polished crystal at incidence 20° , with no reflector, Teflon, ESR coupled with air and ESR coupled with optical grease (clockwise). In contrast to the rough crystal, the distribution of reflected rays is much narrower and centered on the specular reflection for a flat surface (red arrow). The rays reflected by the reflector (green dots) show a much broader distribution for Teflon than ESR (see inset).

For all reflector types, the simulations and experiments showed excellent agreement in relative light output (figure 10(a)). The small overestimation at 18 mm with the ESR reflector is likely explained by the differences in modeling the ESR piece on the top surface of the crystal: the simulations assume ideal contact between the crystal and ESR without any discontinuities, whereas the junction between the top ESR and the ESR on the lateral sides in the experiment will likely lead to a small amount of light leakage, most prominent at the 18 mm position. The simulated maximum light output, taken at 2 mm and normalized by the crystals with no reflector (figure 10(b)), reveals that the simulation overestimated light output by 39% for Teflon and by 25% for the ESR. We partially explain these differences by the coupling of the crystal to the photodetector, which was modeled as ideal in the simulations (see section 3.3). In contrast, the ESR-grease showed a slight (14%) underestimation. We hypothesize that some fraction of the optical grease gets pushed to the sides of the crystal when coupling the photodetector to the crystal, and that this disrupts the crystal-air interface in the case of Teflon and ESR-air, resulting in an overestimation of the simulated light output. Since there is already optical grease present in the case of ESR-grease, this model imperfection is no longer present.

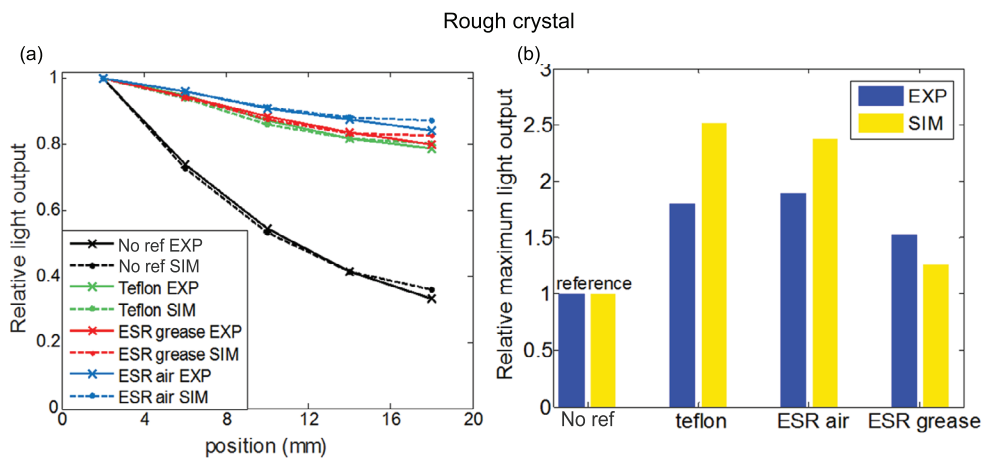


Figure 10. Light output for rough crystals with no reflector, Teflon, or ESR (air-coupled or grease-coupled). (a) The normalized outputs show excellent agreement between experiments (EXP) and simulations (SIM) for all types of reflectors. (b) The maximum light output, taken at the depth closest to the photodetector show reasonable agreement.

The track length of individual photons was recorded and histogrammed independently for the five simulated depths (figure 11). The external reflector strongly lengthened the paths of optical photons: for the bare crystal, even furthest from the photodetector, all track lengths histograms were at most ~ 45 mm, while other configurations showed long tails persisting beyond 70 mm. For ESR and Teflon tape, path lengths showed long tails that extend beyond 150 mm (figure 11, bottom right).

Differences in light output and track length can also be explained by studying the average number of reflections per scintillation photon. The middle column of table 3 shows that using Teflon tape with rough surfaces results in the highest number of reflections (20.8) for the generated scintillation photons which is a 7-fold increase from bare crystals, while coupling ESR with grease decreases this reflection number from 18.9 to 10.2. This again illustrates that direction of the reflected rays strongly affects the reflection pattern and the collection of light. The reflections are given for all generated scintillation photons, which includes both lost and detected photons.

3.2.2. Polished crystals. Simulated light outputs for polished crystals showed good agreement with experimental data (figure 12(a)), with similar variation as a function of irradiation depth. The ESR grease was slightly underestimated in simulations compared to experiments (red curve). Both the experimental and simulated Teflon (in green) showed a minimum between 10 and 14 mm, with an increase at 18 mm, indicating the ability of the model to predict light output with high accuracy. Figure 12(b) shows that the simulated maximum light output is lower than the experimental values, while the rough crystal showed opposite trends. This may be explained by a weaker effect of the crystal-photodetector coupling in polished crystals where the polished surface minimizes the light loss through the sides as shown in section 3.3. The ESR grease only showed a small decrease compared to ESR air (9%), in contrast to rough crystals (47% decrease between ESR air and grease). This is consistent with the angular distributions of reflected photons for ESR air and grease for rough and polished crystals (figures 7 and 9). With the polished surface, these distributions were very similar, while in the rough crystal they dramatically change in the presence of grease.

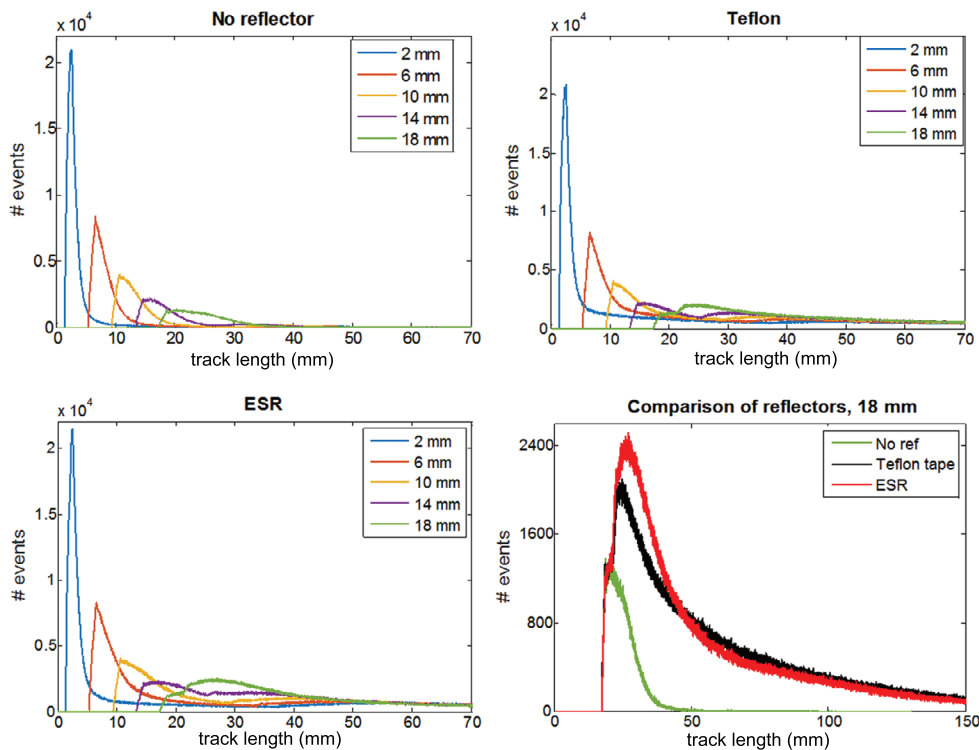


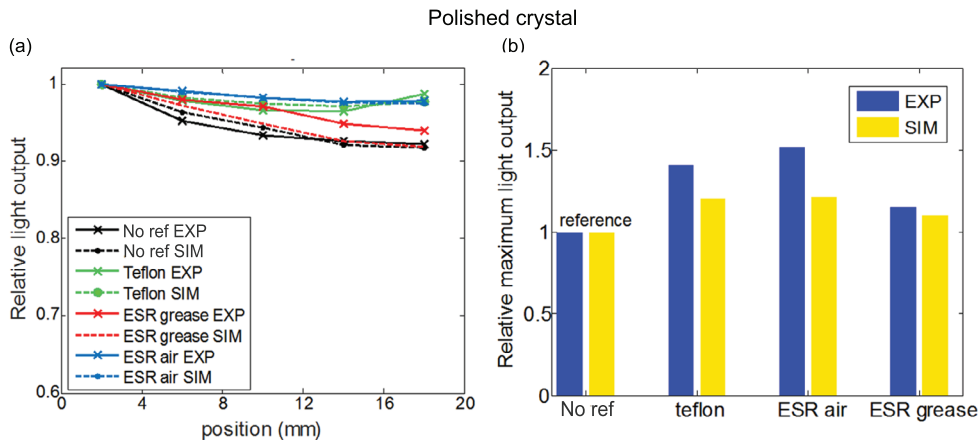
Figure 11. Optical transport in a rough crystal with no reflector, Teflon, or air-coupled ESR (clockwise). Histograms of track length values for all detected photons for emitted at different DOIs show that the presence of a reflector strongly lengthens the transport of optical photons. The bottom right plot illustrates the differences between reflectors.

Table 3, which shows the average number of reflections per generated photon for different surface finish and reflector combinations, further highlights the contrast between rough and polished crystals: the crystal itself when in contact with air, tallies 50.2 reflections/photon when the surface is polished versus 2.8 for a rough surface. Adding Teflon tape or ESR raised the number of reflection/generated photon to more than 60, while coupling the crystal and ESR with optical grease dramatically decreased that number to 13.4. Interestingly, no strong increase in travel distance for the detected photons was observed (figure 13), which suggests that photons undergoing a large number of reflections are ultimately transmitted and not detected.

In contrast to rough crystals in which the presence of a reflector dramatically increased the total travel of individual optical photons, the reflector choice with polished crystals did not substantially affect the total travel length, but did change the shape of the track length histograms (figure 13). When comparing track lengths with no reflector for both crystal finishes, two peaks (corresponding to photons that were initially emitted towards or away from the photodetector) were more clearly visible with the polished crystal (e.g. at 2.5 mm and 46 mm for the 2 mm irradiation depth). The first peak was also narrower in the case of a polished crystal, and showed no tails that were observed for the rough crystal. This can be explained by the wide angular distribution of reflection directions with the rough crystal that randomized the path of the optical photons. The second peak corresponds to the photons that were initially emitted opposite to the photodetector face, and then were reflected back towards it. Plots for ESR and Teflon showed a decrease in the amplitude of the first peak (e.g. -25% for 2 mm irradiation depth) and a related increase in the amplitude of the second

Table 3. Average number of reflections per generated photon.

Reflector	Rough crystal Reflections/photon	Polished crystal Reflections/photon
No ref	2.8	50.2
Teflon tape 4 layers	20.8	61
ESR-air	18.9	66.6
ESR-grease	10.2	13.4

**Figure 12.** Light output for polished crystals with no reflector, Teflon, or ESR (air-coupled or grease-coupled). (a) Normalized outputs for experiments (EXP) and simulations (SIM). (b) Maximum light outputs, taken at the depth closest to the photodetector (2 mm).

peak. Although the second peak started to rise at the same track length (e.g. 38 mm for the 2 mm irradiation depth) for all configurations, there was a very slow increase for a few mm followed by steeper rise to the peak in the absence of reflector. This corresponds to photons that reached the top of the crystal (top face or top of the side faces) and were directly reflected to the photodetector face. The complex shape of the track length histograms arises from several confounding factors, primarily the intersection of the critical angles of each face (Roncali *et al* 2014a).

3.3. Effect of the coupling crystal-photodetector

The analysis of simulated light output data obtained for a rough crystal with Teflon tape or ESR showed an overestimation of the light output (figure 10(b)), though the trend with irradiation depth showed good agreement with experimental data (figure 10(a)). In the simulations, the crystal was always modeled as perfectly coupled to the photodetector, whereas in practice, several factors could degrade the coupling. The first important difference is the probable presence of optical grease on the sides of the crystal, because some amount gets pushed away from the photodetector/crystal contact area when the two surfaces are pressed against each other. This extra optical grease may insert between the crystal and the reflector, dramatically reducing the index mismatch between the crystal and outer medium from the ideal crystal-air interface. In addition, it is well known that Teflon tape is permeable, and that as a result the optical grease will penetrate the Teflon and will decrease its reflectivity. The practical difference between the simulations and experiments is that the reflector is always simulated

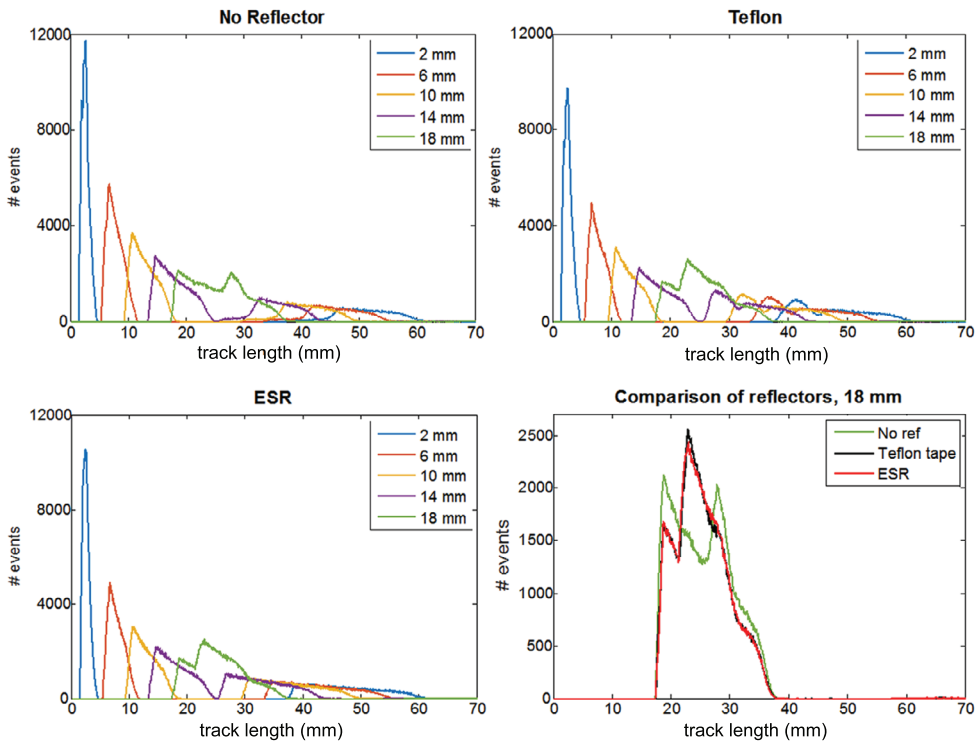


Figure 13. Optical transport in a polished crystal with no reflector, Teflon, or air-coupled ESR (clockwise), for interactions at different DOIs. The reflectors show comparable behavior, and do not lengthen the transport length significantly (bottom right plot).

perfectly aligned with the edge of the crystal, which might not be as flat, with sharp edges, as modeled. There might be a gap between the edge of the reflector material and the edge of the crystal (figure 14). The gap may occur in ESR crystals as well, though ESR is less permeable and its reflectivity is probably not affected by the presence of optical grease. This gap may be in contact with air, or optical grease if it has spread on the sides.

To study these effects we performed simulations for different reflector arrangements (table 4) with a rough and polished crystal finish.

Figure 15(a) shows the maximum light output (at 2 mm from the photodetector face) for all configurations indicated in table 4. The reference is the measured maximum light output at 2 mm, measured with Teflon tape, and then normalized in figure 15. In comparison to the simulated Teflon maximum light output, adding a small gap of 0.2 mm of air or optical grease along the four long sides of the crystal decreased the maximum light output by 5% and 11%, respectively. Artificially decreasing the reflectivity of the Teflon to model penetration by optical grease on 2 mm along the sides of the crystal had a more dramatic decrease and produced a light output comparable to the reference value. While it is not known what the actual decrease in reflectivity is when Teflon is impregnated with optical grease, this result suggests that the coupling crystal-photodetector and resulting imperfections on the sides of the crystal may have a strong effect on the observed light output and can explain the differences between the simulations and measurements with rough crystals. Figure 15(b) shows the same configurations but for a polished crystal, and indicates that the coupling has a weaker effect on the light

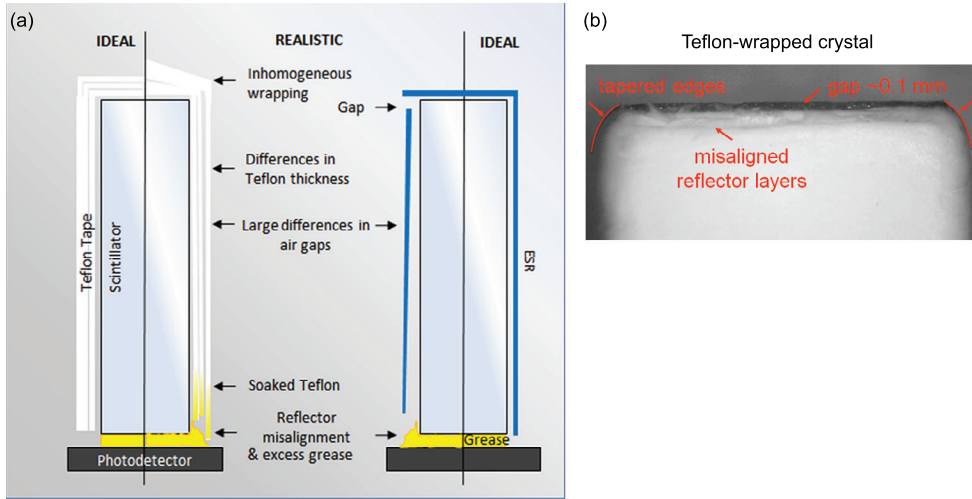


Figure 14. (a) Different scenarios for suboptimal reflector application to the crystal. (b) Microscopic picture of a $3 \times 3 \times 20$ mm³ LSO rough crystal wrapped and used in experiments (side view). Note the tapered edges, the misalignment of some layers, and the small gap at the tip (shown by the red arrows).

Table 4. Practical conditions of coupling crystal/photodetector.

Crystal surface	Coupling (n)	Length (mm)	Reflector (R)
Rough or polished	Air gap	0.2	Teflon 4 layers
	Grease gap	0.2	Teflon 4 layers
	No gap	2	Teflon 4 layers with reflectivity decreased to 75% + grease infiltration

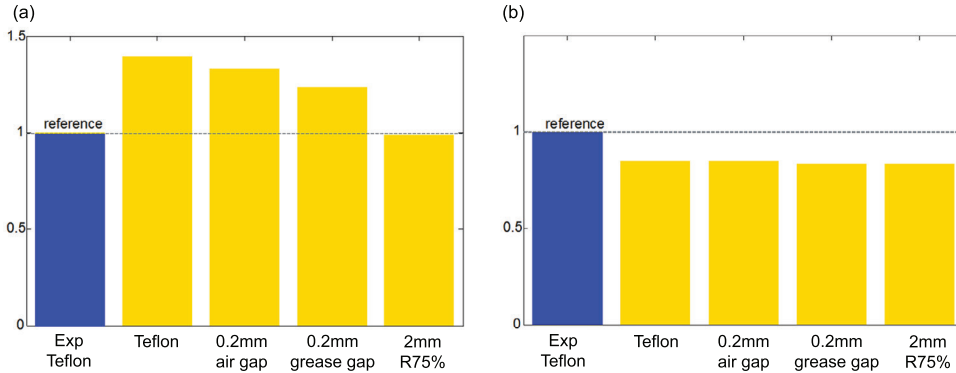


Figure 15. Effect of the crystal coupling to the photodetector on light output for (a) a rough crystal, (b) a polished crystal. All simulations are done with Teflon tape (4 layers, air-coupled).

output, consistent with experimental results. This is likely due to the fact that fewer photons escape the polished surface.

Further explanation regarding the discrepancy between experimental and simulated results is provided in the discussion.

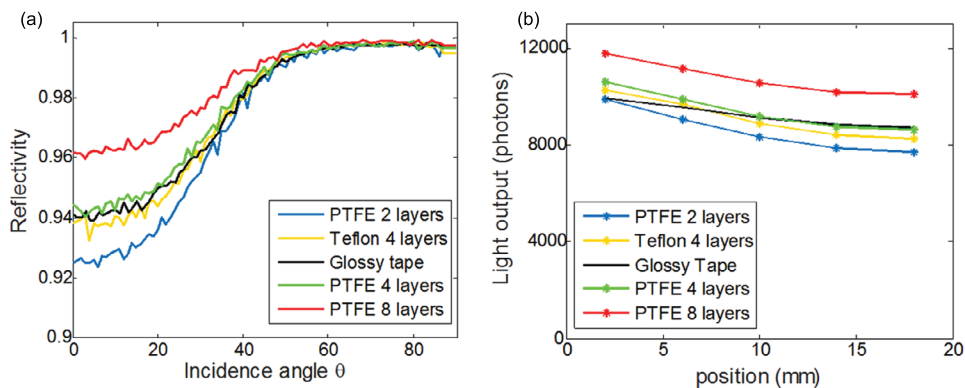


Figure 16. (a) Reflectivity values for PTFE 2–8 wrapping layers and the Teflon used in experiments (air coupling). (b) Resulting light output from 2500 events simulated in the crystal. The light output reflects the variation between the reflectivity curve and show a 20% increase when more layers are used.

3.4. Other reflectors

To illustrate the importance of properly modeling the reflector properties, the light output was also simulated for four other reflectors. Three were Lambertian PTFE tape with different numbers of layers of wrapping (2, 4, and 8) and one reflector was modeled as a glossy tape. Results from the validation simulations performed with the Teflon tape ‘Teflon 4 layers’ (see sections 3.1.1 and 3.2.1) are reported in yellow in figure 16. The reflectivity for PTFE increased with the number of layers (figure 16(a)) at angles of incidence less than $\sim 45^\circ$. While it is expected that increasing the number of layers increases the overall reflectivity, it is interesting to note that 8 layers produced a much higher reflectivity (e.g. 0.96 instead of 0.925 for 2 layers at 0° , as shown in figure 16(a)), which can have a large effect on the photon collection, as photons undergo an average of 21 reflections before being detected. Higher reflectivity with a greater number of reflector layers suggests that trapping of the photons between the layers, which could decrease the reflectivity of such a configuration, was not important. The efficiency of the reflectors was observed in the light output, with a gradual increase with more layers of PTFE (figure 16(b)). The trend as a function of depth did not change between the different PTFE and Teflon materials considered. In contrast, the glossy tape that showed a reflectivity close to that of PTFE 4 layers showed a weaker depth dependency (black curve, figure 16(b)). These results indicate that a user must carefully consider the reflector and its coupling properties when modeling a detector, in order to perform an accurate comparison of light output values and ultimately optimize detector performance.

4. Discussion

In this work, we extended the crystal reflectance model we previously developed to incorporate reflectors attached to the surface. We integrated the crystal and reflector optical properties in a LUT that can be used to accurately model the optical behavior of scintillators in a simulation framework such as GATE. The LUTs that integrate a surface finish and a reflector were used to conduct advanced studies on the effect of the reflector on light output, number of reflections, and travel distance of optical photons in the crystal. These sophisticated LUTs were validated against experimental results and showed good agreement with measured data.

As there is no exact calibration between the number of photons collected in the simulation and the experimental setup, it is necessary to compare relative quantities, such as the difference in light output between different crystal finishes.

The comparison of the normalized light output showed excellent agreement between simulations and experiments at all irradiation depths, indicating that the reflections on the crystal sides were accurately modeled: with 10–20 reflections per photon on average (table 3), significant errors in the modeling of the crystal reflectance would be amplified when the photon ultimately exits the crystal and would be clearly visible. However, when comparing the maximum light output between different configurations, the simulations did not perform as well. Simulation results with the rough crystals showed an overestimation of the predicted light output with Teflon and ESR (air-coupled), which we partially explained with a study of the coupling to the photodetector face and consideration of the imperfections of coupling medium layer on the first few millimeters from the exit face. While it is impossible to exactly model the imperfections in the reflector wrapping in the case of Teflon tape (e.g. variation of layers, air gap between layers, presence of optical grease and subsequent degradation in the reflectivity), this part of the study indicated a strong effect of the coupling efficiency. Another potential source of error well described by (Pauwels *et al* 2012) is the ‘edge effect’ that accounts for small ($\sim 100 \mu\text{m}$) defects at the crystal edges. The authors showed that the light output was strongly affected by adding a scattering region close to the edges of the crystal, and showed the existence of such defects in crystal micrographs. These pictures are consistent with our microscopic observations. In fact, these edge effects might also explain why rough crystals showed overall better accuracy than polished crystals. In the case of rough crystals, the LUT are computed based on AFM data that extend to 1–4 μm depending on the crystal, and account for some of those edge effects by computing the multiple reflections in surface grooves. In contrast, the measured surface of polished crystals is much smoother (table 3) and does not account for larger defects. Polished LUTs therefore do not model this effect at all, which might result in larger discrepancies with experimental light output measurement.

This in fact raises a broader question on the ability of a given crystal finish and reflector model to accurately represent an experimental configuration, and what information can be reliably extracted from such simulations. The effect of the crystal-photodetector coupling study produces an important conclusion for users of such simulation tools: in ideal conditions the simulation is likely to provide reliable/accurate prediction, but in cases where practical experimental laboratory conditions cannot be tightly controlled, variations may result. This is also true for different surface finish conditions that may not be correctly represented by a generic surface model. To address this limitation, we plan to (1) provide a database of various surfaces with precise information on actual roughness, measurement conditions etc to the GATE users, and (2) develop an interface for users to generate their LUTs for their own surfaces when there is a need to represent the exact surface. For users to perform semi-quantitative comparison of various reflectors and surface finishes, there is great value in a well-validated and extended database.

5. Conclusion

We have developed a complete optical model of scintillator surface finishes and reflectors that is packaged in the format of a look-up-table that can be accessed by widely used simulation software such as GATE and Geant4. Our model was validated against experimental data, and applied to study the effect of the reflector and coupling media on optical transport in the crystal. Validated LUTs will be part of the next GATE release in spring 2017, together with modifications in the code to enable the LUT model to be used in lieu of the default Unified

model. Detailed description of the surface finish and reflector optical properties (e.g. roughness average R_a , roughness rms σ , reflectivity spectrum) will be provided with the LUTs for the user to choose a surface representative of their application. In the future, we will also develop an interface for the users to compute their own LUTs, using their scintillator and reflector characteristics.

Acknowledgments

This work was supported in part by NIH grant R03 EB020097 and NIH grant R35 CA197608. E Roncali, M Stockhoff, and S R Cherry are with the Department of Biomedical Engineering, University of California Davis, Davis, CA 95616, USA. The authors also thank Dr Kwon for supporting the experiments, and Dr Berg for reviewing the manuscript and scientific discussions.

References

- Agostinelli S *et al* 2003 Geant4—a simulation toolkit *Nucl. Instrum. Methods Phys. Res. A* **506** 250–303
- Berg E, Roncali E and Cherry S R 2015 Optimizing light transport in scintillation crystals for time-of-flight PET: an experimental and optical Monte Carlo simulation study *Biomed. Opt. Express* **6** 2220–30
- Cuplov V, Buvat I, Pain F and Jan S 2014 Extension of the gate monte-carlo simulation package to model bioluminescence and fluorescence imaging *J. Biomed. Opt.* **19** 026004
- Gundacker S, Auffray E, Pauwels K and Lecoq P 2016 Measurement of intrinsic rise times for various $\text{Lu}(\text{Y})\text{O}_3$ and LuAG scintillators with a general study of prompt photons to achieve 10 ps in TOF-PET *Phys. Med. Biol.* **61** 2802
- Ito M, Lee J S, Park M-J, Sim K-S and Hong S J 2010 Design and simulation of a novel method for determining depth-of-interaction in a PET scintillation crystal array using a single-ended readout by a multi-anode PMT *Phys. Med. Biol.* **55** 3827–41
- Ito M, Lee M S and Lee J S 2013 Continuous depth-of-interaction measurement in a single-layer pixelated crystal array using a single-ended readout *Phys. Med. Biol.* **58** 1269
- Jan S *et al* 2004 Gate: a simulation toolkit for PET and SPECT *Phys. Med. Biol.* **49** 4543–61
- Janecek M 2012 Reflectivity spectra for commonly used reflectors *IEEE Trans. Nucl. Sci.* **59** 490–7
- Janecek M and Moses W W 2008 Optical reflectance measurements for commonly used reflectors *IEEE Trans. Nucl. Sci.* **55** 2432–7
- Janecek M and Moses W W 2009 Measuring light reflectance of BGO crystal surfaces *IEEE Trans. Nucl. Sci.* **55** 2443–9
- Janecek M and Moses W W 2010 Simulating scintillator light collection using measured optical reflectance *IEEE Trans. Nucl. Sci.* **57** 964–70
- Ki-Beom K, Yoon-Heung T, Yoon-Soo H, Kwang-Heum B, Myung-Hee Y and Moon-Ho L 2003 Relationship between surface roughness of indium tin oxide and leakage current of organic light-emitting diode *Japan. J. Appl. Phys.* **42** L438
- Kwon S I, Ferri A, Gola A, Berg E, Piemonte C, Cherry S R and Roncali E 2016 Reaching 200 ps timing resolution in a time-of-flight and depth-of-interaction positron emission tomography detector using phosphor-coated crystals and high-density silicon photomultipliers *JMI* **3** 043501
- Lecoq P 2012 New approaches to improve timing resolution in scintillators *IEEE Trans. Nucl. Sci.* **59** 2313–8
- Levin A and Moisan C 1996 A more physical approach to model the surface treatment of scintillation counters and its implementation into DETECT *IEEE Nuclear Science Symp. Conf. Record* pp 702–6
- Loignon-Houle F, Bergeron M, Pepin C M, Charlebois S A and Lecomte R 2015 Simulation of signal losses in highly pixelated scintillator arrays read out by discrete photodetectors *2015 IEEE Nuclear Science Symp. and Medical Imaging Conf. (NSS/MIC)* pp 1–3
- Melcher C L and Schweitzer J S 1992 Cerium-doped lutetium oxyorthosilicate—a fast, efficient new scintillator *IEEE Trans. Nucl. Sci.* **39** 502–5

- Nemallapudi M V, Gundacker S, Lecoq P, Auffray E, Ferri A, Gola A and Piemonte C 2015 Sub-100 ps coincidence time resolution for positron emission tomography with LSO:Ce codoped with Ca *Phys. Med. Biol.* **60** 4635
- Park H 2012 Optics of vikuiti films
- Pauwels K, Auffray E, Gundacker S, Knapitsch A and Lecoq P 2012 Effect of aspect ratio on the light output of scintillators *IEEE Trans. Nucl. Sci.* **59** 2340–5
- Pizzichemi M et al 2012 Ray tracing simulations in scintillators: a comparison between SLITRANI and geant4 2012 *IEEE Nuclear Science Symp. and Medical Imaging Conf. Record (NSS/MIC)* pp 1712–6
- Ren S, Yang Y and Cherry S R 2014 Effects of reflector and crystal surface on the performance of a depth-encoding PET detector with dual-ended readout *Med. Phys.* **41** 072503
- Roncali E and Cherry S R 2013 Simulation of light transport in scintillators based on 3D characterization of crystal surfaces *Phys. Med. Biol.* **58** 2185–98
- Roncali E, Kim C L, McDaniel D L, Bircher C and Cherry S R 2014a Effect of angular distribution and collection of scintillation photons on PET detectors timing resolution *IEEE NSS/MIC (Seattle)*
- Roncali E, Viswanath V and Cherry S R 2014b Design considerations for DOI-encoding PET detectors using phosphor-coated crystals *IEEE Trans. Nucl. Sci.* **61** 1–7
- Seifert S, Steenbergen J H L, Dam H T V and Schaart D R 2012 Accurate measurement of the rise and decay times of fast scintillators with solid state photon counters *J. Instrum.* **7** P09004
- Weele D N t, Schaart D R and Dorenbos P 2015 Picosecond time resolved studies of photon transport inside scintillators *IEEE Trans. Nucl. Sci.* **62** 1961–71
- Yang Y, Dokhale P A, Silverman R W, Shah K S, McClish M A, Farrell R, Entine G and Cherry S R 2006 Depth of interaction resolution measurements for a high resolution PET detector using position sensitive avalanche photodiodes *Phys. Med. Biol.* **51** 2131–42